A New Echocardiographic Model for Quantifying Three-Dimensional Endocardial Surface Area

DAVID E. GUYER, MD, FACC, THOMAS C. GIBSON, MB, FACC, LINDA D. GILLAM, MD, FACC,

MARY ETTA KING, MD, GERARD T. WILKINS, MB, CHB, J. LUIS GUERRERO,

ARTHUR E. WEYMAN, MD, FACC

Boston, Massachusetts

A new technique for quantitatively mapping the three-dimensional left ventricular endocardial surface was developed, using measurements from standard cross-sectional echocardiographic images. To validate the accuracy of this echocardiographic mapping technique in an animal model, the endocardial areas of 15 excised canine ventricles were calculated using measurements made from echocardiographic studies of the hearts and compared with areas determined with latex casts of the same ventricles. Close correlation ($r = 0.87$, $p < 0.001$) between these two measures of endocardial area provided preliminary confirmation of the accuracy of the maps.

To further characterize the mapping algorithm, it was translated into computer format and used to map the surfaces of idealized hemiellipsoids. Areas measured with this mapping technique closely approximated the actual areas of idealized surfaces with a wide spectrum of shapes; maps were particularly accurate for ellipsoids with shapes similar to those of undistorted human ventricles. Also, the accuracies of area calculations were relatively insensitive to deviation from the assumed positions of the echocardiographic short-axis planes. Finally, although the accuracy of the mapping technique improved as data from more transverse planes were added, the procedure proved reliable for estimating surface areas when data from only three planes were used. These studies confirm the accuracy of the echocardiographic mapping technique, and they suggest that the resulting planar plots might be useful as templates for localizing and quantifying the overall extent of abnormal wall motion.

(*J Am Coll Cardiol 1986;8:819–29*)

In patients with ischemic heart disease, the extent of regional dysfunction is a major determinant of overall left ventricular performance (1–3). Accordingly, the ability to quantify both the total endocardial surface area and the area of segmental dysfunction has significant clinical and research applications. Contrast ventriculography is the current standard for measuring both overall ventricular size and area of segmental dysfunction. However, the risks associated with cardiac catheterization and contrast dye injections prevent their use in all but a small subset of potential patients of interest, and restrict serial follow-up studies. Furthermore, angio-graphic techniques visualize only those walls that form a border with the cardiac blood pool, and so they are limited by geometric assumptions used to calculate endocardial areas from ventriculographic images.

Cross-sectional echocardiography is unique among available cardiac imaging techniques in enabling tomographic views of the heart to be obtained in multiple orthogonal planes that are readily standardized by reference to internal cardiac landmarks (4). As a result, an echocardiographic examination provides information about the three-dimensional structure and function of the entire left ventricle. Until now, however, there has been no readily applicable method for combining data from multiple echocardiographic imaging planes to measure and graphically display left ventricular endocardial areas.

In this report we introduce a new echocardiographic mapping technique that enables calculation of total endocardial surface area using data from standard cross-sectional studies. Maps derived using this technique display the smoothed endocardial surface of the left ventricle in an easily visualized planar format, and should provide the framework for

quantifying the global extent of abnormal wall motion in patients with ischemic heart disease.

The purpose of this study was to verify that this new mapping technique measures total endocardial surface area accurately. To achieve this, the accuracy of the mapping technique was validated in comparison with two independent methods for determining ventricular surface area. First, endocardial areas derived from hand-drawn echocardiographic maps of a group of excised canine hearts were compared with the experimentally measured smoothed endocardial surface areas of the same hearts. In the second phase, a computer-based study was performed using the mapping technique to map a series of hemiellipsoidal surfaces with lengths similar to those of the human left ventricle and to compare the map areas of those figures with their calculated actual surface areas.

Methods

Geometric Principles Underlying the Echocardiographic Mapping Technique

The algorithm or calculation procedure for mapping the ventricular endocardial surface which is described here was derived from the following concepts: 1) If the endocardial surface of a left ventricle was hypothetically coated with a thin liner, then the area of the liner would correspond to the endocardial surface area of the ventricle. 2) If the left ventricle was then sectioned into four quadrants using two mutually perpendicular apex to base cuts, these two cuts would also quadrisect the thin ventricular liner. 3) If the four sections of the liner that resulted from two such apex to base cuts of the ventricle were separated from the endocardial surface and laid flat, they would form a two-dimensional map of the endocardial surface. This is analogous to making a planar map of the terrestial globe. The length of each section or quadrant of the ventricular map would then roughly correspond to the length of the ventricle, and the curved edges of each quadrant to the sectioned edges of the liner; the width of each section at any position along the central or long axis would correspond to one-fourth of the ventricular endocardial circumference at that level.

Figure 1A is a schematic representation of such a left ventricular liner, and shows the general dimensions that serve to define the shape and size of the liner and, hence, of the endocardial surface area. The first dimension is the central apex to base long-axis length (labeled L_{ax}), and is the distance from the apical point to the center of the basal plane. Although this dimension does not actually appear on an endocardial map, it does help to define the size and shape of the endocardial surface and is used as the starting point in the iterative mapping procedure (described later). The second dimension is the endocardial apex to base segment length (labeled SL in Figure 1A), which can be defined as
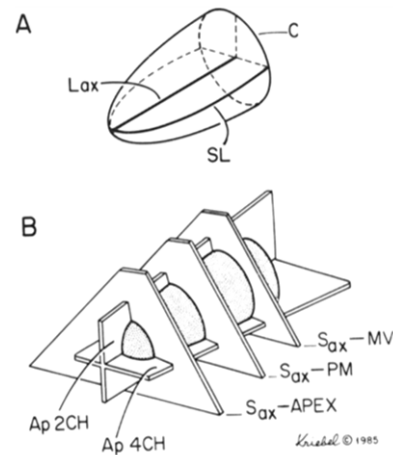

Figure 1. A, Schematic liner of the left ventricular cavity with representative dimensions used to plot endocardial maps. **B,** Relative positions of echocardiographic imaging planes shown as they intersect a left ventricle or ventricular liner. Ap 4CH = apical four chamber plane; Ap 2CH = apical two chamber plane; C = short-axis circumference; Lax = central long axis of the liner; S_{ax}-APEX = apical short-axis plane; S_{ax}-MV = mitral value short-axis plane (see text); S_{ax}-PM = papillary muscle short-axis plane; SL = apex to base endocardial segment length.
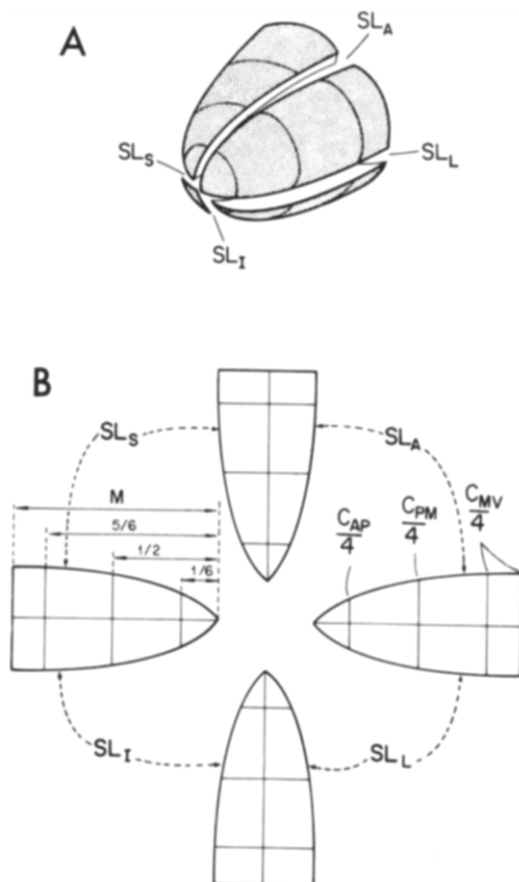
one of the family of shortest curved segments running from the apical point to the base of the liner along the surface of the liner. A pair of these curved endocardial segments is determined by the intersection of any plane that includes the central ventricular axis with the liner. The length of each segment is roughly one-half of the total curved segment resulting from the intersection of the plane and the liner. Finally, short-axis circumferences (one of which is labeled C in Fig. 1A) are the dimensions that result when the liner is transected by any plane perpendicular to its long axis.

Figure 1B illustrates how standard echocardiographic imaging planes intersecting a representative ventricle yield dimensions that correspond to those required to describe the area of the ventricular liner in Figure 1A. Comparable dimensions of the ventricle are derived from images taken in these planes in the following ways. The long-axis length of the ventricle (L_{ax}) is defined as the greatest distance from the apical endocardium to the center of the mitral anular plane in either the apical two or four chamber view. Four endocardial apex to base segment lengths are measured: those from the lateral wall and septal wall are determined in the apical four chamber view, and those from the anterior wall and inferior wall in the apical two chamber plane. Short-axis imaging planes are shown at the mitral valve (S_{ax}-MV) and midpapillary muscle (S_{ax}-PM) levels, and at an apical level just below the papillary muscles (S_{ax}-APEX). Short-axis circumferences (C) are measured at each of these levels by tracing the endocardial border.

The quadrants of an idealized left ventricular liner that results from its division by two perpendicular apex to base

cuts are shown in Figure 2A. A planar map of the endo-cardial surface results when the four quadrants are laid flat. Such a map can be reconstructed using the measurements taken from echocardiographic images of the heart. Figure 2B shows how ventricular dimensions measured from the standard imaging planes of the echocardiographic study de-scribed earlier would appear on an endocardial map. It is important to note again that the long-axis (or L_{ax}) dimension does not appear on an endocardial map. This central axis of the ventricle runs down the center of the cavity and does not lie along the endocardial surface. Rather, a midline dimension of each quadrant (M) is the distance from the apical tip to the basal plane of the map that does appear on the maps. This dimension M is not measured directly from

the echocardiographic images, but is determined by the map-ping procedure using a technique of successive approxi-mations.

The morphologic assumptions that underlie the construc-tion of these plots from routine echocardiographic mea-surements relate to the positions at which imaging planes intersect the endocardial surface. It is assumed that the apical short-axis imaging plane intersects the central ventricular axis one-sixth of the way from apex to base. Likewise, the midpapillary muscle short-axis plane is assumed to intersect the ventricular long axis half way along its length, and the mitral valve plane is assumed to intersect the central axis five-sixths of the way from the apex to the base of the ventricle. These positions are all based on the assumption that each of the three short-axis planes lies centrally within its respective anatomic third of the ventricle, as defined by Edwards et al. (5). The effect of deviations from these assumed plane positions upon the accuracy of the mapping technique was tested as described later. Finally, it is as-sumed that the endocardial short-axis circumference at the base of the ventricle is substantially the same as the cir-cumference at the mitral valve level.

Figure 2. A, Schematic diagram of endocardial liner that has been quadrisected by two perpendicular apex to base cuts. The trans-verse lines represent the positions at which short-axis planes would intersect the liner. **B,** A representative endocardial map resulting from the flattening of the four quadrants of a liner, as shown in **A.** The dimensions of the liner are shown as they would be on the map. C_{AP} = endocardial short-axis circumference at the apical level; C_{MV} = circumference at mitral valve level (see text); C_{PM} = circumference at midpapillary muscle level; M = map quadrant midline dimension; SL_A = anterior wall endocardial segment length; SL_I = inferior endocardial segment length; SL_L = lateral wall endocardial length; SL_S = septal endocardial apex to base segment length.

Comparison of Echocardiographic Mapping-Derived Endocardial Area With Measured Area

Echocardiographic data collection. To validate the mapping technique, the formalin-fixed hearts of 17 mongrel dogs were immersed in a water bath, and echocardiographic images were obtained with an ATL Mark III mechanical sector scanner (Advanced Technology Laboratories). A 5 MHz transducer was used for each study. The echocardio-grams were recorded on 0.5 inch (1.27 cm) magnetic tape using a Panasonic NV-8200 VHS video recorder (Matsush-ita Electric Industrial Co., Ltd.).

Two orthogonal views equivalent to the standard apical four and two chamber planes were recorded for each heart. The apical four chamber equivalent view was defined by placing the transducer over the lateral left ventricular wall, rather than at the apex, and adjusting the scan plane so that it intersected both the mitral and tricuspid anuli at their widest diameters. The true ventricular apex was located by maximizing the long-axis dimension of the images. The apical two-chamber equivalent plane was then defined by rotating the ventricle 90° about its long axis so that all right-sided cardiac structures were excluded from the echocar-diographic image. The position of the ventricle was adjusted so that the imaging plane intersected the base of the left ventricle at its widest diameter, and the ventricular long-axis length was again maximized by making fine adjust-ments in transducer angulation. Apical-equivalent images employ the axial resolution of the imaging system to opti-mize visualization of the water-myocardium interface. Rep-
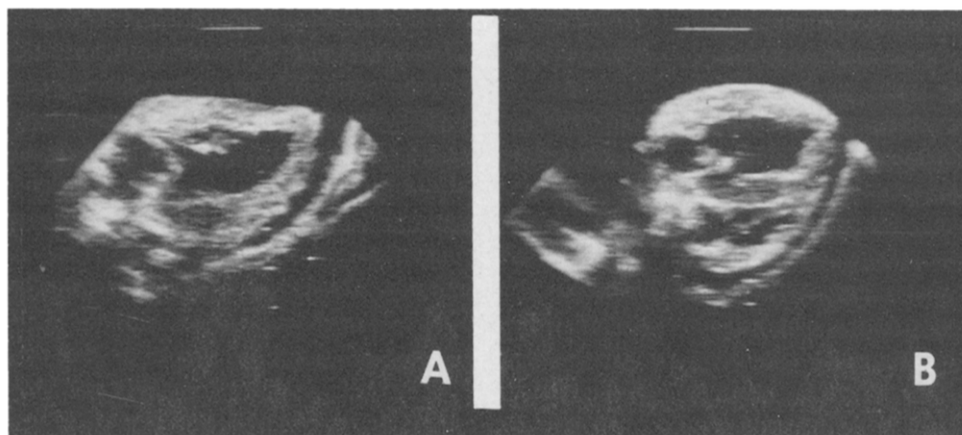
Figure 3. Representative apical equivalent images of excised dog heart in a water bath. **A,** Apical two chamber view; **B,** apical four chamber view.

resentative apical two and four chamber images from one of the dogs are shown in Figure 3.

Short-axis views were obtained for each heart by positioning the transducer above the anterior wall and adjusting the scan plane to minimize both the horizontal and the vertical obliquity in the images of the left ventricular cavity. Short-axis images at the mitral valve, midpapillary muscle and apical levels are shown in Figure 4. The locations of these short-axis planes were standardized using internal ventricular landmarks: the mitral valve leaflets, the papillary muscles and the ventricle just below the papillary muscles.

Echocardiographic data analysis. Videotapes containing the echocardiographic data were reviewed using an off-line analysis system (Easy View II, Microsonics Inc.). Frames with optimal image quality were transferred to a video disc system for the measurement of ventricular dimensions. Data for the construction of ventricular maps were then obtained as follows: The ventricular long-axis length was measured in either of the two apical-equivalent views described. Where discrepancies occurred, the long-axis length was taken as the average of the measurements from the two views. Apex to base endocardial segment lengths were measured by tracing the inner edge of the endocardial surface from the tip of the cardiac apex to the base of the ventricle in each of two mutually perpendicular apical views. The ventricular circumferences were measured by tracing the endocardial border at each of the three short-axis levels. All dimensions were determined from three separate frames, and the results for each dimension were averaged to obtain a single value.

To construct the maps from available echocardiographic data, the quadrant midline dimension (M) was plotted along each of the four major axes of a planar Cartesian coordinate system ($+X$, $-X$, $+Y$, $-Y$) (Fig. 5A). These segments formed the spines of the four map quadrants. For the first stage in the mapping procedure (iteration 1), the M dimen-

sion was assumed to be the measured left ventricular long-axis length (L_{ax}).

The three short-axis circumferences were then divided by 4, and the resulting segment lengths plotted on each of the long axes at their appropriate positions, so that they were perpendicular to and bisected by the quadrant midlines. Figure 5B shows a map completed to this point, with the midlines and short-axis arms laid out. Then, the apical point and the ends of the short-axis arms of each quadrant were connected with a smooth curve using a draftsman's plastic spline (Fig. 5C). The lengths of the resulting four curved endocardial apex to base segments from the map were then measured on a digitizing pad and compared with the corresponding endocardial segment lengths measured in the apical echocardiographic images.

Map adjustment. If the endocardial segment lengths from the mapping procedure were within predetermined tolerance specifications of the echocardiographic endocardial segment lengths, the map was complete. In many cases, however, there was a small difference between the two values, and so the map was adjusted by increasing or decreasing the quadrant midline dimension (M) and repeating the entire plotting sequence using the same short-axis circumferences. A flow diagram of this iterative algorithm is shown in Figure 6. In this study, the midline dimension (M) of the previous iteration was incremented by the difference between the map and the echocardiographically measured endocardial segment lengths to obtain the next iterations's midline dimension (M) value:

$$M[i + 1] = M[i] + (SL_{echo} - SL_{map}[i]), \qquad (1)$$

where the [i] index denotes the value of a given map dimension from the ith map iteration, and *where* M[1] is equal to the ventricular long-axis length (L_{ax}).

With this method of adjusting the quadrant midline dimension the map endocardial segment lengths converged rapidly to the measured values, and it was never necessary to make more than two iterations to meet the tolerance
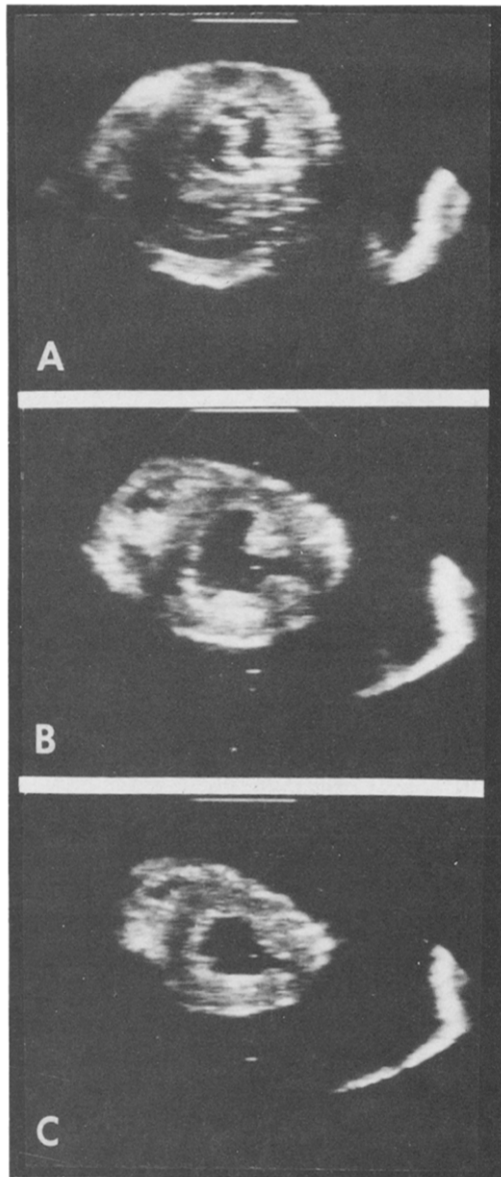
Figure 4. Short-axis echocardiographic images of one excised dog heart taken at the mitral valve (A), midpapillary muscle (B) and apical (C) levels.
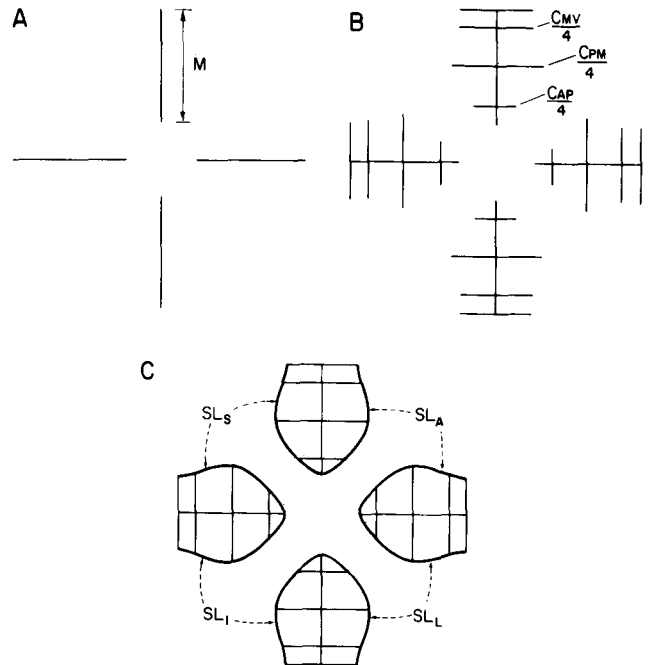

Figure 5. Procedure for plotting an endocardial map from echocardiographic data. A, Quadrant midline dimensions are laid out. In the first stage, the plotting sequence, the ventricular long-axis dimension is used as the map quadrant midline (M) value. B, Short-axis data are then plotted at their correct positions along the quadrant midlines. C, Smooth curves are fitted between the ends of the short-axis arms and the apex points of each quadrant. Abbreviations as in Figure 2.

specifications of 5% for the hand-calculated maps. In addition, the convergence properties of this iterative technique were tested empirically using the computerized algorithm to be described. The initial value of the map quadrant midline dimension was varied from 0.1 to 100 times the measured ventricular long-axis dimension, and in all cases the algorithm converged within three iterations to the same area value.

After plotting was completed, the map-derived endocardial area of each heart was determined by planimetry of the four map quadrants on a calibrated digitizing pad. The estimates of total endocardial areas from the hand-drawn maps were then compared with directly measured smoothed endocardial surface areas.

Determination of smoothed endocardial surface area.

Water was drained from each ventricle after completion of its echocardiographic study, and the cavity was then filled through the mitral orifice with a silicone rubber molding compound (Microfil, Canton Bio-Medical Products, Inc.). When the silicone rubber had cured (typically overnight), the resulting ventricular mold was carefully dissected free of the surrounding myocardium, lubricated with petroleum jelly, and painted with five coats of a latex molding compound (Pliatex Mold Rubber, Sculpture Products and Accessories). The dried latex cast was then incised and peeled off the mold. It was pinned flat with a minimum of distortion, and its outline was traced onto paper. The area of the latex mold was measured by planimetry of the tracing. This experimentally determined area was deemed to be the smoothed endocardial surface area for comparison with the corresponding area derived by the echocardiographic mapping technique.

Computer Analysis of Distortions Resulting From Echocardiographic Mapping of Idealized Left Ventricles

Computer programs. Because comparison of endocardial areas described is at best approximate and the nature of the mapping procedure makes iterative hand calculations
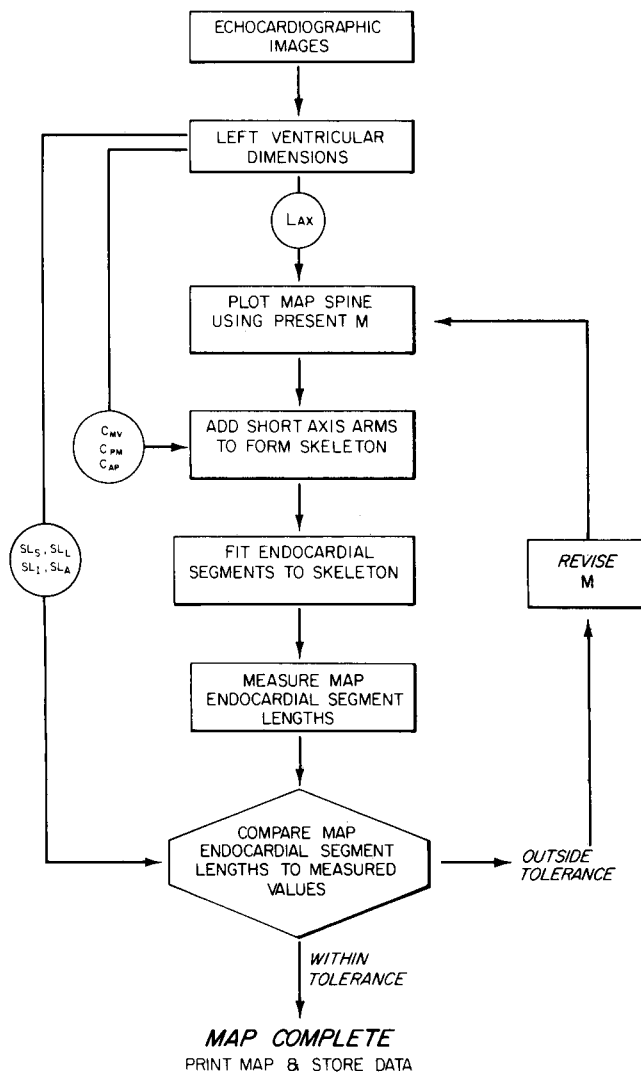
Figure 6. Steps in the iterative mapping procedure, or algorithm, for plotting endocardial surface maps. Abbreviations as in Figures 1 and 2.

time consuming, we developed two interactive computer programs: 1) The first permitted us to construct hemiellipsoid surfaces of various sizes and shapes, and to calculate a precise surface area for each. These surfaces were chosen on the assumption that the contracting portion of an undistorted human ventricle has a nearly hemiellipsoid configuration. 2) The second program automated the endocardial mapping algorithm using measurements derived from the idealized hemiellipsoid surfaces generated by the first computer program. A map-derived area was then calculated by the second program. The accuracy of the mapping technique, therefore, was tested by comparing the map areas with the actual areas of the hemiellipsoid surfaces. Furthermore, we were able to determine the theoretical effects of varying the apex to base locations of the short-axis plane and of incrementing the amount of input measurement data

obtained by additional short-axis cuts on the accuracy of map areas.

Computer implementation of the echocardiographic mapping algorithm. A prolate ellipsoid, also known as a prolate spheroid, is the three-dimensional figure that results from the rotation of an ellipse about its major or longer axis. A hemiellipsoid is formed when an ellipsoid is bisected by a plane perpendicular to its long axis. The shape of a hemiellipsoid is determined by the lengths of its semimajor axis (A) and semiminor axis (B), or by the eccentricity (e):

$$e = \sqrt{\frac{A^2 - B^2}{A^2}} \qquad (2)$$

The first computer program generated a series of hemiellipsoid surfaces in the following manner. Input data consisted of the eccentricity and semimajor axis length, which allowed the program to define the exact shape and size of each surface. The program then generated the appropriate dimensions of the hemiellipsoid needed to produce a map of its surface using the mapping algorithm. These dimensions were: 1) the apex to base or long-axis length (L_{ax}), equal to the ellipsoid semimajor axis; 2) apex to base segment lengths (SL), each equal to one-fourth of the circumference of the ellipse of revolution; and 3) short-axis circumferences (C), equal to the circumferences of the circles that result when the ellipsoid is sliced transversely by planes perpendicular to its major axis at various points along that axis. The program was designed to generate values for circumferences at as few as 3 to as many as 20 short-axis transverse planes. The number of such circumferences and their locations along the long axis were specified by the program user.

The second computer program, the mapping program, was based on the algorithm diagrammed in Figure 6, and it utilized the ellipsoid dimensions generated by the first program. The computer constructed maps in the manner of the hand-drawn maps in the first part of this validation study by laying out a map skeleton and then connecting the end points of the skeleton with curved segments (Fig. 5C) to produce map-derived endocardial segment lengths. Any mathematical procedure for connecting the skeleton end points could be inserted in the program. In the present computer implementation, the program connected adjacent points on the skeleton with parabolic arcs. As with the hand-drawn maps, the comparison between map and true endocardial apex to base segment lengths was used to test for accuracy of the maps. This computer program required the map endocardial segment length to be within 1% of the ellipsoidal dimension. If the map segment lengths did not meet these specifications, the quadrant midline dimension (M) was adjusted as was done for the hand-drawn maps (see equation [1]), and the iterative plotting procedure was repeated. When a map was complete, its area was computer-calculated by

numerical integration and compared with the surface area of the idealized hemiellipsoid, whose true value was calculated by the first computer program (6).

Validation of the computer program. The computer programs, written in the programming language PASCAL, were run on a VAX 11/780 digital computer (Digital Corporation). Initial data of known results were entered to test the output of the major subroutines of the programs. These checks verified that this program calculated accurate ellipsoid endocardial segment lengths and surface areas, and that its map areas corresponded to the areas of the hand-drawn maps. Figure 7 shows the relation between the hand-drawn and computer-derived map areas of 14 hemiellipsoids with different sizes and shapes. The same ellipsoid dimensions were used for both techniques of map construction. These and all other preliminary computer runs confirmed the accuracy of the program's calculations under a variety of input data conditions.

Distortion calculations. The computer program was then used to derive endocardial maps for a series of hemiellipsoid surfaces with a fixed long-axis dimension and with eccentricities varying from 0.0 (hemispherical) to 0.9999 (long, narrow ellipsoids). A long-axis dimension of 8.0 cm was selected for this experiment because it is approximately the average value for adult human ventricles (7). For each ventricular shape (eccentricity) the program produced a map using short-axis data from 3 to 10 planes. The ratio of the map area to the true ellipsoid area was calculated for each combination of ventricular shape and number of short-axis planes. This ratio is a measure of the overall distortion produced by the mapping procedure. An area ratio of 1.0 represents no overall distortion in a map's estimate of endocardial area, while ratios between 0 and 1 represent under-

estimations and ratios greater than 1 are overestimations by the mapping procedure relative to the true endocardial area.

To determine the potential effects of shifts of short-axis plane positions from their assumed apex to base locations on the accuracy of map-derived areas, short-axis circumference data were varied systematically. The hemiellipsoid surface was divided into thirds along the central long axis and each of the thirds was further subdivided into 10 equally spaced segments. As described previously, the mapping algorithm assumes that the short-axis circumferences are measured at the midpoint of each third of the ventricle. The short-axis circumference of the midventricular and basal thirds were calculated for those midpoints of those thirds, and circumferences for each of the 10 apical thirds levels were used to plot a separate map. This entire process was repeated two more times, each time holding the short-axis circumference at two levels constant while varying the circumference of the third. Once again, for each of the combinations of short-axis data, the accuracy of the mapping technique was determined as the ratio of map to true hemiellipsoid surface area.

Results

Comparison of echocardiographic map areas with smoothed endocardial areas: excised canine left ventricles. Construction of endocardial maps using data from echocardiographic images was possible in all 17 excised dog hearts. However, latex casts for measurements of endocardial areas were constructed for only 15 of the 17 hearts because the friable silicone rubber ventricular molds could not be excised from the hearts of two dogs. The areas of

Figure 7. Comparison of map-derived surface areas of ellipsoid surfaces from hand-drawn (**abscissa**) and computer-drawn (**ordinate**) endocardial maps. The dimensions used to plot the maps by the two procedures were the same for each surface.
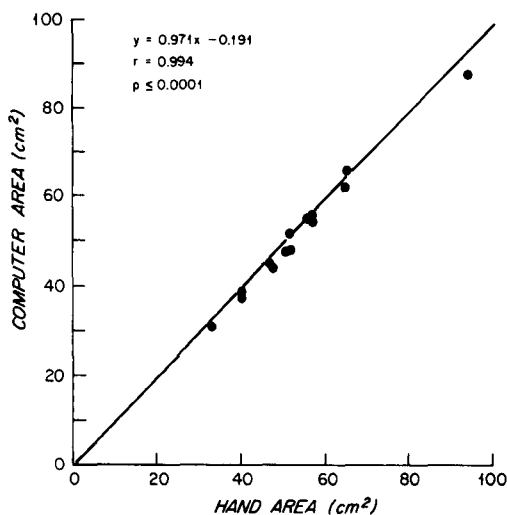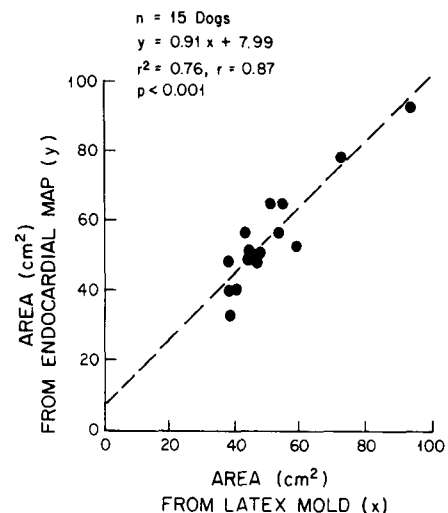

Figure 8. Correlation of endocardial surface areas derived from endocardial maps (**ordinate**) with smoothed surface areas calculated from latex molds (**abscissa**) of 15 excised canine ventricles. The **dashed line** represents the line of least regression; there is a definite tendency for the map areas to overestimate latex areas.

the smoothed endocardial surfaces of the remaining 15 hearts were compared with their corresponding map areas.

The comparison of map areas to smoothed endocardial areas is shown graphically in Figure 8. The correlation coefficient between the two estimates of area is 0.87 in this series, which is significant at the p < 0.001 level. Map areas from the largest hearts closely approximate the smoothed endocardial areas. In smaller hearts, however, there is more variability in the relation between these two measures of endocardial area, with map areas generally overestimating the corresponding smoothed areas determined from the latex casts.

Calculation of the distortion in mapping idealized hemiellipsoid surfaces. The ratios of map-derived areas to true ellipsoid surface areas are shown in Table 1. It is evident that the mapping algorithm is accurate in quantifying the surface areas of the hemiellipsoids. The largest error is a 7.6% underestimation (0.924 ratio) of hemispherical areas by maps using short-axis circumference data from three planes (row 1, column 3). Map estimates rapidly approach true areas as the ellipsoid eccentricity approaches 1.0. Figure 9 is a plot of the area ratio as a function of the ellipsoid eccentricity when three short-axis circumferences are used to plot the maps.

At eccentricities of 0.7 and 0.99 there are interruptions in the steady increase of area ratios. These occur at transition points in the number of iterations required to bring

the segment length dimensions within tolerance. With eccentricities between 0.0 and 0.6, three iterations were required to meet endocardial segment length specifications. For eccentricity values between 0.7 and 0.98, two iterations were needed. Beyond an eccentricity of 0.98, a single calculation brought the map and true endocardial segment lengths within the tolerance specification. However, inspection of both Table 1 and Figure 9 reveals that, although magnified by the scale on the graph, the actual decrease in area ratio is small at both transition points.

The data in Table 1 show that, for any given eccentricity, increasing the number of transverse or short-axis planes improves the accuracy of a map's estimate of hemiellipsoid area. This can be seen graphically in Figure 10, where the area ratio is plotted against the number of short-axis planes used to define the endocardial map of a hemiellipsoid with an eccentricity of 0.95, selected because this shape lies within the physiologic range for undistorted ventricles. However, although increasing the number of planes does improve the area ratio, the maximal overall increase resulting from the use of 10 imaging planes as compared with 3 is only 1.2% with this ventricular shape. Almost all of the improvement results as the number of planes is increased from three to six, and there is virtually no further increase in the area ratio when more than six planes are used.

The effects of varying the short-axis plane positions within their respective thirds of a hemiellipsoid ventricle on the

Table 1. Ratios of Map-Derived to Actual Areas of Ellipsoid Surfaces With Varying Shapes (eccentricities) and Using Transverse Plane Data From 3 to 10 Levels

Eccentricity	True area (cm²)	Number of Short-Axis Planes							
		3	4	5	6	7	8	9	10
0.0000	402.12	0.924	0.928	0.930	0.931	0.932	0.932	0.932	0.933
0.1000	399.44	0.925	0.929	0.930	0.932	0.932	0.933	0.933	0.933
0.2000	391.36	0.926	0.930	0.932	0.933	0.934	0.934	0.934	0.935
0.3000	377.77	0.929	0.933	0.935	0.936	0.936	0.937	0.937	0.937
0.4000	358.47	0.933	0.936	0.938	0.940	0.940	0.941	0.941	0.941
0.5000	333.14	0.938	0.942	0.944	0.945	0.945	0.946	0.946	0.946
0.6000	301.19	0.944	0.948	0.950	0.951	0.952	0.952	0.953	0.953
0.7000	261.59	0.942	0.946	0.948	0.950	0.950	0.951	0.951	0.952
0.8000	212.22	0.955	0.960	0.962	0.964	0.964	0.965	0.965	0.966
0.9000	147.24	0.971	0.976	0.979	0.980	0.981	0.982	0.982	0.983
0.9100	139.29	0.973	0.978	0.981	0.982	0.983	0.984	0.984	0.985
0.9200	130.93	0.975	0.980	0.983	0.984	0.985	0.986	0.986	0.987
0.9300	122.08	0.976	0.982	0.984	0.986	0.987	0.988	0.988	0.988
0.9400	112.63	0.978	0.984	0.986	0.988	0.989	0.990	0.990	0.990
0.9500	102.42	0.980	0.985	0.988	0.990	0.991	0.991	0.992	0.992
0.9600	91.24	0.981	0.987	0.990	0.991	0.992	0.993	0.994	0.994
0.9700	78.66	0.983	0.988	0.991	0.993	0.994	0.995	0.995	0.996
0.9800	63.91	0.984	0.990	0.993	0.994	0.996	0.996	0.997	0.997
0.9900	44.95	0.977	0.982	0.985	0.987	0.988	0.989	0.989	0.990
0.9990	14.13	0.984	0.990	0.993	0.995	0.996	0.997	0.997	0.997
0.9999	4.47	0.985	0.991	0.994	0.996	0.997	0.998	0.998	0.998

Each row represents data for one shape or eccentricity that is indicated in column 1. The second column lists the actual or true areas of the hemiellipsoids, and succeeding columns display the area ratios (map area/true area) of the surfaces using transverse or short-axis circumferences from 3 to 10 planes. The actual hemiellipsoid areas are calculated for surfaces with semimajor axis lengths of 8.0 cm.
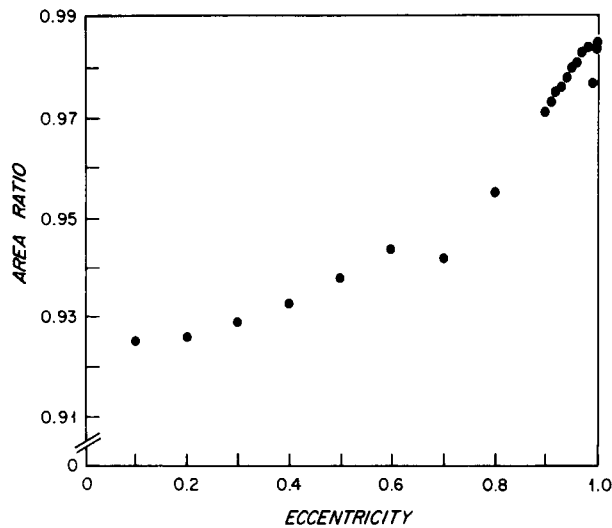
Figure 9. Relation of the area ratio (endocardial map area/true ellipsoid area) (**ordinate**) to the eccentricity (**abscissa**) of the ellipsoid surface being mapped. These data are derived from Table 1, and represent the use of three transverse planes.

area ratio are shown in Figure 11. Once again, the data for this graph were derived from a hemiellipsoid with an eccentricity of 0.95. It is obvious that moving a short-axis plane to a more basal position increases the area ratio. This effect is most marked for deviations in the apical short-axis position, and least so for the mitral valve plane.

Figure 10. Effect of increasing the number of transverse circumferences used to plot endocardial surface maps of idealized ellipsoid surfaces. This is analogous to increasing the number of short-axis planes at which echocardiographic images are recorded and dimensions measured for plotting maps of actual ventricles.
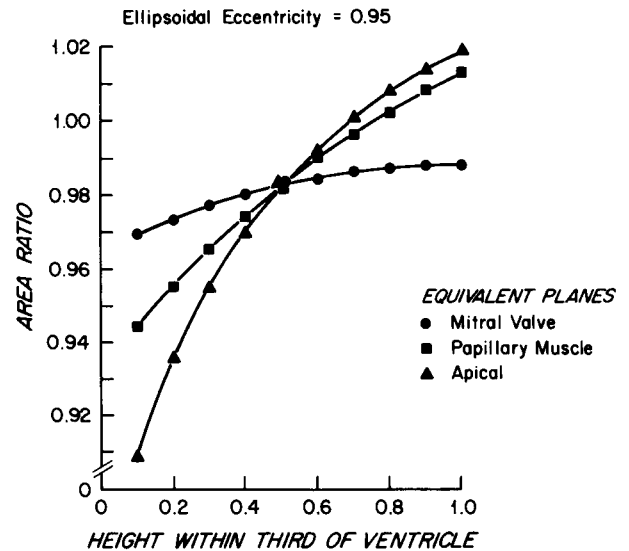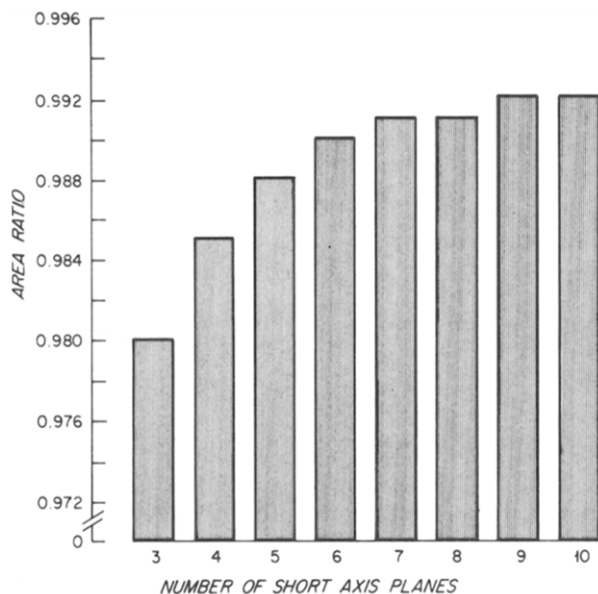

Figure 11. Effect of varying the relative apex to base position of each short-axis plane on overall accuracy of the map. The horizontal axis represents the height at which the short-axis circumference was measured within the appropriate third of the ventricle, with 0.1 being 1/10 of the way from the most apical extreme of the given third to the base. The position of the two short-axis planes that are not varied is the correct one: each halfway along its respective third of the central long axis. The relative position of the variable plane within its third of the ventricle is plotted along the **abscissa** (see text).

Discussion

In this report, we have described and validated a new technique for measuring and graphically displaying the smoothed endocardial surface of the left ventricle using readily available echocardiographic data. Estimates of total endocardial area have previously been used as a basis for calculating the extent of abnormal wall motion in patients with segmental left ventricular dysfunction and determining the effects of such wall motion abnormalities on overall ventricular performance (1–3,8,9). Because of the complex three-dimensional structure of the left ventricle, however, most such models have assumed the endocardial surface to be spherical, an assumption that incorrectly describes the true ventricular shape and precludes adaptation to changes in ventricular contour. The echocardiographic mapping technique described in this study is free of major assumptions about ventricular shape and in the undistorted hearts we tested has been shown to accurately describe endocardial surface area. It should therefore provide a useful template on which to display segmental ventricular function and against which to compare changes in regional and global left ventricular size.

Validation of Echocardiographic Mapping Technique

Comparison with measurements of excised ventricles. In the development of any system such as the echocardiographic mapping technique, it is important first to validate

the accuracy of the concepts on which the technique is based and from this to determine the sources and limitations of the methods. Validation of this new technique took place in two phases. In the first phase, we compared areas of maps derived from actual echocardiographic measurements taken from in vitro recordings of excised hearts with the areas of thin rubber casts replicating those endocardial surfaces. The resulting data suggest that the mapping technique overestimates the endocardial surface areas of smaller canine ventricles while correlating almost exactly with the areas of larger ventricles.

The differences in the measured areas of the smaller ventricles could result from errors in the echocardiographic measurements, mapping technique or area measurements of the latex casts of the endocardial surface. Errors in the echocardiographic measurements are well recognized and relate to the point spread function inherent in both the axial and lateral resolving characteristics of all echocardiographic systems (4). These artifacts, however, should result in an underestimation in ventricular dimensions, and hence area, rather than the overestimation noted in this study. A systematic error introduced by the mapping technique itself might likewise lead to over- or underestimation of the measured volumes. However, such an error would be expected to occur in all area calculations. Because our data suggest that for larger ventricles the map areas are virtually identical to measured areas, this explanation does not appear to account for the size-related differences that were noted.

The third possible cause, and the one that we believe most likely explains the observed overestimation, results from a fundamental limitation in the method used for measuring endocardial surface areas of the excised ventricles. Because the latex casts replicate the endocardial surface in both overall shape and regional topography, they contain all of the trabecular infoldings of the endocardium. These irregularities, combined with the recognized distortion encountered when flattening a roughly hemiellipsoid figure onto a planar surface, made it extremely difficult to lay the casts from smaller hearts completely flat. As a result, the smoothed endocardial areas measured with the latex casts, in all likelihood, underestimate true ventricular areas, and the resulting errors are larger with the smaller hearts. This conclusion is further supported when the raw echocardiographic dimensions are compared with the same measurements taken from tracings of the latex casts. The mean circumferences at the mitral valve and papillary muscle levels uniformly overestimated measurements taken from the latex casts at the same levels. However, because adult human hearts at end-diastole should be comparable in size with the larger dog hearts in this study, we would expect the accuracy of the echocardiographic technique in mapping human ventricles to correspond more closely to that observed with the larger hearts examined here. Endocardial areas from end-systolic maps of human left ventricles might

have the same overestimation errors that were found in the smaller canine ventricles.

Comparison with computer simulation. Although there was good correlation between map areas and the measurement of endocardial area in the initial phase of this validation study, there were clear limitations in these comparisons that prevented us from rigorously testing the accuracy of the assumptions inherent in the mapping algorithm. As a result, we developed a computer simulation in which hemiellipsoid surfaces with known sizes, shapes and areas could be generated and to which the mapping algorithm could then be applied in order to compare map areas with the known areas of the idealized surfaces more precisely. This more rigorous comparison suggested that the mapping algorithm is extremely accurate in calculating the areas of hemiellipsoids, although it underestimates actual areas by small amounts. At ellipsoid eccentricities corresponding to those encountered in the normal human ventricle (0.94 to 0.96, using normal data from Triulzi et al. (7)), the degree of underestimation varied from 0.8% using data from 10 short-axis planes to 2% using three planes. As the generated figures became more hemispherical, the degree of underestimation increased to a maximal theoretic error of approximately 7%. At the extremes of what would be considered physiologic, however, (that is, an eccentricity of approximately 0.80), the underestimation was only 4.5% with three planes. This suggests that 5% would be the largest error in clinical studies due to the mapping algorithm alone.

The cause of this underestimation appears to lie in one of the major assumptions of the mapping algorithm, specifically that the three echocardiographic short-axis planes intersect the map leaf axes at roughly one-sixth, one-half and five-sixths of their apex to base lengths. This approximation is based on morphologic data that indicate that these relations are appropriate relative to the central long axis of an undistorted ventricle (5). Some error is clearly introduced with this plane positioning because, for example, a short-axis plane halfway along the central ventricular long axis will not be halfway along the endocardial segment because of the nonuniform apex to base curvature of the endocardial surface. The shift in relative short-axis position is most pronounced for hemispherical surfaces, where the greatest underestimation of areas occurs, and least for the more eccentric ellipsoid surfaces, where the smallest errors in area calculations were found. Although the resulting errors are obviously small, if desirable it should be relatively easy to introduce a shape-related correction factor to adjust the map estimates of area based on the overall shape of the particular ventricle being plotted.

Further computed analysis of the mapping technique showed that its accuracy in calculating the areas of the hemiellipsoids improved as data from increasing numbers of short-axis planes were used. However, the improvement resulting from the use of additional planes was small in

these idealized chambers. These data are analogous to those of Weiss et al. (10), who studied the effect of varying numbers of short-axis echocardiographic planes on Simpson's rule calculations of ventricular volumes. Their study indicated that in undistorted hearts, accurate left ventricular volumes can be calculated from measurements taken at as few as four short-axis echocardiographic sections. Likewise, we found that the maximal improvement in area estimation occurred when a fourth short-axis plane was added (we did not examine the accuracy of using only one or two planes). Virtually no improvement resulted from the use of six or more short-axis planes.

Distortions produced by the planar transformation of curved endocardial surfaces are not evenly distributed over such surfaces. Thus, an analysis of the localized effects of the algorithm is needed to fully characterize the mapping technique. Such an analysis is a complex problem of three-dimensional geometry that is only now being approached. However, the small errors found in the preceding analysis lead to the preliminary conclusion that this mapping technique will not be hindered by excessive localized distortions.

Clinical Applications

Because the maps are derived from readily available echocardiographic data, they are, by design, applicable to clinical studies and are currently used for this purpose in our laboratory. On the basis of the computer validation data presented here, it appears that the map areas slightly underestimate ventricular areas. Indeed, errors for ventricles of approximately human size are so small that they should be virtually undetectable.

The point spread function of all echocardiographic systems may result in further slight underestimations of true areas where measurements are derived from clinical images. This problem is encountered in all clinical applications of echocardiography, but it has not limited the usefulness of the technique. Further, when the mapping technique is applied to large populations, the resulting data should be internally consistent.

Although internal cardiac landmarks allow the echocardiographer to appropriately position the three standard short-axis planes with some degree of confidence (4), a certain amount of variation in the exact apex to base location of these planes is to be expected in clinical studies. Fortunately, the data plotted in Figure 11 indicate that the accuracy of the mapping algorithm is not very sensitive to exact plane positioning. Inaccuracies in the mitral plane position have almost no effect on the area ratio. The other two short-axis planes affect the area ratio to a larger extent, although the magnitude is still quite small.

The results presented here relate only to symmetric ventricles. The position of the three short-axis planes may be

altered more dramatically in aneurysmal ventricles. Although we have not yet studied the use of the mapping technique with distorted ventricles, it should be possible to identify the apex to base locations of the short-axis planes from apical echocardiographic images of such hearts and make appropriate adjustments in the algorithm.

Conclusion. The mapping technique outlined in this study uses data from routine echocardiographic images to produce accurate planar representations of the smoothed left ventricular surface. This echocardiographic mapping technique assumes that the endocardium can be treated as if it were a thin membrane which, when quadrisected by two mutually perpendicular apex to base planes, can be laid flat with a minimum of distortion. As currently formulated, this technique uses ventricular dimensions from two orthogonal apical views and at least three short-axis echocardiographic imaging planes in an iterative algorithm. Agreement between measured endocardial segment lengths and the corresponding map-derived dimensions provides the end point for this algorithm. The iterative nature of the technique causes the resulting endocardial surface maps to conform to the left ventricular configuration, and the resulting map areas have been demonstrated to correlate closely with both measured and theoretical ventricular surface areas.

References

1. Vayo HW. The theory of the left ventricular aneurysm. Bull Math Biophys 1966;28:363–70.

2. Klein MD, Herman MV, Gorlin R. A hemodynamic study of left ventricular aneurysm. Circulation 1967;35:614–30.

3. Swan HJC, Forrester JB, Diamond G, Chatterjee K, Parmley WW. Hemodynamic spectrum of myocardial infarction and cardiogenic shock. Circulation 1972;45:1097–1110.

4. Weyman AE. Cross-sectional Echocardiography. Philadelphia: Lea & Febiger, 1982:98–135.

5. Edwards WD, Tajik AJ, Seward JB. Standardized nomenclature and anatomic basis for regional tomographic analysis of the heart. Mayo Clin Proc 1981;56:479–97.

6. Beyer WH, ed. CRC Standard Mathematical Tables. 26th ed. Boca Raton, Florida: CRC Press, 1973:129.

7. Triulzi MO, Gillam LD, Gentile F, Newell JB, Weyman AE. Normal adult cross-sectional echocardiographic values: linear dimensions and chamber areas. Echocardiography 1984;1:403–26.

8. Crawford DW, Barndt R, Harrison EC, Lau FYK. A model for estimating some of the effects of aneurysm resection following myocardial infarction: preliminary clinical confirmation. Chest 1971;59:517–23.

9. Kitamura S, Echevarria M, Kay JH, et al. Left ventricular performance before and after removal of the non-contractile area of the left ventricle and revascularization of the myocardium. Circulation 1972;45:1005–17.

10. Weiss JL, Eaton LW, Kallman CH, Maughan WL. Accuracy of volume determination by two-dimensional echocardiography: defining requirements under controlled conditions in the ejecting canine left ventricle. Circulation 1983;67:889–95.